

# A Least Squares based Groupwise Image Registration Technique

Nefeli Lamprinou, Nikolaos Nikolikos and Emmanouil Z. Psarakis<sup>1</sup>

*Computer Engineering and Informatics Department, Patras, Greece*


**Keywords:** Groupwise Registration, Congealign, Image Alignment, Medical Imaging, Multi-modal Alignment, Self Quotient Image.

**Abstract:** Compared with pairwise registration, groupwise registration is capable of handling a large-scale population of images simultaneously in an unbiased way. In this work we improve upon the state-of-the-art pixel-level, Least-Squares (LS) based groupwise image registration methods. Specifically, we propose a new iterative algorithm which outperforms in terms of its computational cost, a recently introduced LS based iterative congealing scheme. Namely, the particle system that was introduced in that work is used and by imposing its “center of mass” to be motionless, during each iteration of the minimization process, a sequence of “centroid” images whose limit is the unknown “mean” image is optimally in closed form defined, thus solving in a reduced computational cost the groupwise problem. Moreover, the registration technique is properly adapted by the use of Self Quotient Images (SQI) in order to become capable for solving the groupwise registration of multimodal images. Since the proposed congealing technique is invariant to the size of the image set, it can be used for the successful solution of the problem on large image sets with low complexity. From the application of the proposed technique on a series of experiments for the groupwise registration of face, unimodal and multimodal magnetic resonance image sets its performance seems to be very good.

## 1 INTRODUCTION

The problem of image congealing or groupwise alignment/registration is an important one within the computer vision community. A good congealing algorithm can be used as preprocessing to notably improve the performance of other vision tasks within different research areas (Liu and Wang, 2014). Compared to the pairwise registration, groupwise registration is capable of handling a large-scale population of images simultaneously in an unbiased way. Specifically, it eliminates the requirement of choosing a reference image, thus avoiding a registration bias. Our work improves upon the most widely recognized area based LS based state-of-the-art approach. Most area based state-of-the-art algorithms can be considered (Nikolikos et al., 2017) as variations of a common base framework. The basic idea is to use one image at a time as the held out image and the rest of the ensemble as the stack. Having done that the goal is to minimize, in an iterative fashion, an error function defined over all of the ensemble, by estimating a warp update for the held out image that aligns it with the stack. Algorithms based on the aforementioned

idea include groupwise methods with entropy based cost functions, such as the algorithms proposed in (Learned-Miller, 2006), (Zollei, 2006), (Vedaldi and Soatto, 2006) as well as with LS based cost functions such as the methods proposed in (Cox et al., 2008), (Cox et al., 2009), (Cox, 2010), (Xue and Liu, 2012). In (Storer and Urschler, 2010) an error function based on mutual information that copes with possible variations in appearance between similar objects of the same class is defined. In addition, in (Huang et al., 2007) and (Huang et al., 2012) extended entropy based congealing for the usage on real world complex images is proposed. Recently, in (Huizinga et al., 2016), (Guyader et al., 2018) groupwise registration techniques were tailored for the registration of quantitative MRI datasets. LS based congealing algorithms tend to perform better in terms of convergence rate and accuracy. In the LS case, there are two ways to align the held out image with the stack using gradient descend optimization techniques. The first one, which is known as the forward LS congealing approach has poor alignment performance, especially for strong initial misalignments, but has a really low computational cost. On the other hand the inverse LS congealing approach that computes a common warp

<sup>1</sup>  <https://orcid.org/0000-0002-9627-0640>

update for all images of the stack by utilizing the inverse approach presented in (Cox et al., 2008) outperforms the forward LS in both accuracy and robustness, but its high computational cost, due to existing nested loops, makes its use prohibitive for large image sets as the number of sub-problems grows quadratically with respect to the image set's size. Moreover, additional robustification is needed in order to be able to handle outliers (Cox, 2010).

The proposed groupwise method improves upon all the desirable characteristics of the state-of-the-art inverse method, while maintaining a linear to the set size computational cost, similar to that of the forward approach. Moreover, the proposed technique is computationally cheaper than its predecessor (Nikolikos et al., 2017) where, in each iteration of the algorithm, the singular value decomposition of the pseudo inverse of the Jacobian matrices over the entire ensemble of the images was needed. Finally, the proposed technique, as well as its predecessor, can be easily adapted to make use of feature descriptors, instead of intensity values, as the representation of each image, as the majority of the unsupervised intensity-based techniques during the joint alignment process do, in order to cope with background variations.

The remainder of this paper is organized as follows: In Section 2, we formulate the image congealing problem and several issues related with it are examined. In Section 3, the particle system that was introduced in (Nikolikos et al., 2017) that is strongly related to the geometric transformations of the image's set is reviewed, and the proposed optimal definition of the "centroid" image is presented. In Section 4, the results of the experiments we have conducted are presented. Finally, Section 5 concludes our paper.

## 2 PROBLEM FORMULATION

### 2.1 Preliminaries

Let us consider a set containing  $N$  images:

$$\mathbb{S}_i = \{\mathbf{i}_n\}_{n=1}^N \quad (1)$$

that belong to the same cluster, that is  $\mathbb{S}_i$  contains a group of similar in shape and aligned images, where  $\mathbf{i}$  denotes the column-wise of length  $N_x N_y$  vectorized version of size  $N_x \times N_y$  image  $I$ . Then, it is well known that the "mean" image which is defined by:

$$\bar{\mathbf{i}}^* = \frac{1}{N} \sum_{n=1}^N \mathbf{i}_n \quad (2)$$

constitutes the most representative image for the cluster and it can result from the solution of the following

optimization problem:

$$\bar{\mathbf{i}}^* = \arg \min_{\bar{\mathbf{i}} \in \mathbb{R}^{N_x N_y}} \left\{ \sum_{n=1}^N \|\bar{\mathbf{i}} - \mathbf{i}_n\|_2^2 \right\} \quad (3)$$

where  $\|\mathbf{x}\|_2$  denotes the  $l_2$  norm of vector  $\mathbf{x}$ . Let us now consider, apart from the set  $\mathbb{S}_i$ , the following set:

$$\mathbb{S}_{i_w}(\mathbb{P}) = \{\mathbf{i}_w(\mathbf{p}_n)\}_{n=1}^N \quad (4)$$

containing the geometrically distorted vectorized images of set  $\mathbb{S}_i$  of (1) where

$$\mathbb{P} = \{\mathbf{p}_n\}_{n=1}^N, \quad (5)$$

is a set of  $N$  warp parameter vectors. Under the used warping transformation  $w(\cdot; \mathbf{p}_n)$ <sup>1</sup>, which is parameterized by the vector  $\mathbf{p}_n \in \mathbb{R}^M$ , each pixel  $\mathbf{x}$  of the Region of Interest of image  $\mathbf{i}_n$  of set  $\mathbb{S}_i$  is mapped onto the pixel  $\hat{\mathbf{x}}$  of the corresponding image  $\mathbf{i}_w(\mathbf{p}_n)$  of set  $\mathbb{S}_{i_w}(\mathbb{P})$ , i.e.:

$$I_w(\hat{\mathbf{x}}; \mathbf{p}_n) = I_n(w(\mathbf{x}; \mathbf{p}_n)). \quad (6)$$

In other words the set  $\mathbb{S}_{i_w}(\mathbb{P})$  is generated by the following process:

$$\left. \begin{array}{l} \mathbf{i}_1 \xrightarrow{w(\cdot; \mathbf{p}_1)} \mathbf{i}_w(\mathbf{p}_1) \\ \mathbf{i}_2 \xrightarrow{w(\cdot; \mathbf{p}_2)} \mathbf{i}_w(\mathbf{p}_2) \\ \vdots \\ \mathbf{i}_N \xrightarrow{w(\cdot; \mathbf{p}_N)} \mathbf{i}_w(\mathbf{p}_N) \end{array} \right\} \equiv \mathbb{S}_{i_w}(\mathbb{P}) \quad (7)$$

where, as it was already mentioned, all images belong to the same cluster, are aligned and the "mean" image is defined by (2).

Then, congealing, or groupwise registration (Liu and Wang, 2014) can be defined as the minimization problem of a misalignment function, let us denote it by  $\mathcal{E}(\mathbb{P})$ , which is calculated over the set  $\mathbb{S}_{i_w}(\mathbb{P})$ , for a warping function that models the parametric form of the misalignment to be removed. In general, solving the image congealing problem is not an easy task and its complexity heavily depends on several factors, such as the size of the ensemble and the strongness of the geometric distortions, to name a few.

Although, in some cases the aforementioned problem can be easily solved (Nikolikos et al., 2017), in the general case, its solution results in a highly nonlinear and computationally demanding procedure. This is basically because the goal of estimating the collection of the unknown parameters should be achieved by defining a misalignment function  $\mathcal{E}(\mathbb{P})$  over the entire ensemble of images. Such a function, which is

<sup>1</sup>In this paper, to model the warping process we are going to use the class of affine transformations with  $\mathbf{p}_n \in \mathbb{R}^6$ .

known as the Cumulative Squared Misalignment Error (CSME):

$$\mathcal{E}(\mathbb{P}) = \sum_{n=1}^N \varepsilon(\mathbf{p}_n) \quad (8)$$

where

$$\varepsilon(\mathbf{p}_n) = \sum_{m=1, m \neq n}^N \|\mathbf{i}_w(\mathbf{p}_n) - \mathbf{i}_w(\mathbf{p}_m)\|_2^2, \quad (9)$$

has all these characteristics and was proposed in (Cox et al., 2008). However, since the above total cost function is difficult to be optimized directly (Tong et al., 2009), the iterative minimization of the individual cost function  $\varepsilon(\mathbf{p}_n)$  for each geometrically distorted image  $\mathbf{i}_w(\mathbf{p}_m)$ , given an initial estimation of the warping parameter  $\mathbf{p}_m$ ,  $m = 1, 2, \dots, N$ , was proposed.

In general, aligning each image of the aforementioned set with a stack of images, results in a problem which is heavily depended on the initial conditions of the average image. This is obvious since independently of the blurriness of the basis images, the average image before the alignment of images is blurred. Thus, using the average image to control the direction of the corrections of the parameters, with all the fine details of the image lost, the algorithm is at the mercy of the initial conditions (Cox et al., 2008). In order to avoid this undesired effect, LS congealing avoids using the mean image and for improving the quality of the alignment an inverse compositional LS congealing algorithm was proposed.

However, in the next section we are going to explore ways of obtaining the alignment of the ensemble in (4) without having to align all the individual pairs resulting from it. Instead, we are going to align each image with the “mean” image, which we are going to relate with the “centre of mass” of the geometric transformations set (5).

## 2.2 A Simplified Misalignment Function

In (Nikolikos et al., 2017) the following total mean misalignment function:

$$\mathcal{E}_0(\mathbb{P}; \bar{\mathbf{i}}^*) = \frac{1}{N} \sum_{n=1}^N \|\bar{\mathbf{i}}^* - \mathbf{i}_w(\mathbf{p}_n)\|_2^2 \quad (10)$$

where  $\bar{\mathbf{i}}^*$  denotes the unknown “mean” image, was proposed. It is clear that the above proposed misalignment function is separable, but is a non linear function of each member of the set of warp parameters defined in (5). Thus, for each one of the cost functions involved into (10) its minimization requires non-linear optimization techniques either by using direct search or by following gradient-based approaches. As

is customary in iterative techniques, the original optimization problem is replaced by a sequence of secondary optimizations. Each secondary optimization relies on the outcome of its predecessor, thus generating a chain of parameter estimates which hopefully converges to the desired optimizing vector. At each iteration, we do not have to optimize the objective function but an approximation to this function. Assuming that at the  $k$ -th iteration of the iterative procedure  $\mathbf{p}_n(k)$  is “close” to some nominal parameter vector  $\tilde{\mathbf{p}}_n$ , then we write  $\mathbf{p}_n(k) = \tilde{\mathbf{p}}_n + \Delta\mathbf{p}_n(k)$ , where  $\Delta\mathbf{p}_n(k)$  denotes a vector of perturbations. We recall here that in order to be able to compute the optimal perturbations  $\Delta\mathbf{p}_n(k)$ , the nominal parameter vector  $\tilde{\mathbf{p}}_n$  as well as the “mean” image  $\bar{\mathbf{i}}^*$  must be known. By assigning to the nominal parameter vector  $\tilde{\mathbf{p}}_n$  the estimation of the previous iteration, i.e.:  $\mathbf{p}_n(k-1) \rightarrow \tilde{\mathbf{p}}_n$ , the optimal perturbations can be computed as follows:

$$\Delta\mathbf{p}_n(k) = A_w(\mathbf{p}_n(k-1))(\bar{\mathbf{i}}^* - \mathbf{i}_w(\mathbf{p}_n(k-1))) \quad (11)$$

where

$$A_w(\tilde{\mathbf{p}}_n(k-1)) = (G_w(\tilde{\mathbf{p}}_n(k-1))^T G_w(\tilde{\mathbf{p}}_n(k-1)))^{-1} G_w(\tilde{\mathbf{p}}_n(k-1))^T \quad (12)$$

is the  $M \times N_x N_y$  pseudo inverse of the Jacobian matrix  $G_w(\tilde{\mathbf{p}}_n(k-1))$  evaluated at  $\tilde{\mathbf{p}}_n(k-1)$ , (Baker and Matthews, 2004).

Note however, that since the “mean” image  $\bar{\mathbf{i}}^*$  is unknown the optimal values of the perturbations in (11) can not be computed. Moreover, the use of the following average of the warped vectorized images:

$$\bar{\mathbf{i}}_w(k) = \frac{1}{N} \sum_{n=1}^N \mathbf{i}_w(\mathbf{p}_n(k-1)) \quad (13)$$

leading to a similar approach with the forward one, will have a poor alignment performance (Cox, 2010). In order to overcome this obstacle, in (Nikolikos et al., 2017) a particle system was defined and the motion of each particle was explicitly related with the estimated values of a corresponding parameter vector during the iterative procedure of the optimization. We are going to review this particle system and use it to optimally define, through a new optimization problem the “centroid” vectorized image.

## 2.3 The Particle System

Let us consider that each member of set  $\mathbb{S}_{\mathbf{i}_w}(\mathbb{P})$  denotes the starting position of a particle of mass  $m = 1/N$  that can be moved into  $\mathbb{R}^M$ . Hence the set  $\mathbb{S}_{\mathbf{i}_w}(\mathbb{P})$  could be considered as a set containing the starting positions of a system of  $N$  isobaric particles. Let  $\mathbf{p}_n(k)$  be the position of the  $n$ -th particle at the  $k$ -th

instant as it moves into  $\mathbb{R}^M$ . Then, its trajectory can be defined with the following position's set:

$$\mathbb{T}_n = \{\mathbf{p}_n(k), k = 0, 1, 2, \dots\}, \quad (14)$$

with its first and last element  $\mathbf{p}_n(0)$ ,  $\lim_{k \rightarrow \infty} \mathbf{p}_n(k)$  denoting its starting and ending position respectively and its motion, can be easily expressed by the following simple motion model:

$$\mathbf{p}_n(k) = \mathbf{p}_n(k-1) + \Delta \mathbf{p}_n(k), k = 1, 2, \dots, \quad (15)$$

with the vector  $\Delta \mathbf{p}_n(k)$  denoting its differential movement.

The position of the center of mass of the whole particle system, at the  $k$ -th instant:

$$\bar{\mathbf{p}}(k) = \frac{1}{N} \sum_{n=1}^N \mathbf{p}_n(k) \quad (16)$$

can be used as the origin of the moving coordinate system. Specifically, the position of the  $n$ -th particle at the  $k$ -th instant with respect to the new origin  $\bar{\mathbf{p}}(k)$  can be expressed as follows:

$$\mathbf{p}_n(k) = \bar{\mathbf{p}}(k) + \mathbf{q}_n(k), k = 1, 2, \dots. \quad (17)$$

Note that the vectors  $\mathbf{q}_n(k)$ ,  $n = 1, 2, \dots, N$  denote the positions of the particles in the new coordinate system and are zero mean, that is:

$$\sum_{n=1}^N \mathbf{q}_n(k) = 0. \quad (18)$$

As the optimization (time) goes on, the position vectors of the particles change with time and thus, in general, the center of mass moves too with its velocity given by:

$$\Delta \bar{\mathbf{p}}(k) = \bar{\mathbf{p}}(k) - \bar{\mathbf{p}}(k-1) = \frac{1}{N} \sum_{n=1}^N \Delta \mathbf{p}_n(k) \quad (19)$$

where  $\bar{\mathbf{p}}(k)$ ,  $\bar{\mathbf{p}}(k-1)$ ,  $k = 1, 2, \dots$  are the center of mass of the  $N$ -sized particle system at two consecutive instances. Then, according to *Proposition 3.1* in (Nikolikos et al., 2017), the mean geometric transformation remains the same over the iteration process, i.e.:

$$\bar{\mathbf{p}} = \bar{\mathbf{p}}(k), k = 0, 1, \dots \quad (20)$$

if the total momentum of the particle system is zero, that is:

$$\Delta \bar{\mathbf{p}}(k) = 0. \quad (21)$$

This transformation totally specifies the geometric deformation of the "mean" image and we are going to use it in the next section for defining the "centroid" image.

## 2.4 The "Centroid" Image

To this end, let us define a sequence of vectorized images:

$$\mathbb{I}_c = \{\mathbf{i}(k)\}_{k=1}^{\infty}, \quad (22)$$

having the following two properties (Nikolikos et al., 2017):

- $\mathcal{P}_1$ : The  $k$ -th member of the sequence, is the "centroid" image of the corresponding iteration of the minimization process
- $\mathcal{P}_2$ : The limit of the sequence is the unknown "mean" image, that is:

$$\lim_{k \rightarrow \infty} \mathbf{i}(k) = \bar{\mathbf{i}}^*, \quad (23)$$

and the following average quantities:

$$A(k) = \frac{1}{N} \sum_{n=1}^N A_w(\mathbf{p}_n(k-1)) \quad (24)$$

$$\mathbf{b}(k) = \frac{1}{N} \sum_{n=1}^N A_w(\mathbf{p}_n(k-1)) \mathbf{i}_w(\mathbf{p}_n(k-1)) \quad (25)$$

$$\Delta \bar{\mathbf{p}}(k) = \frac{1}{N} \sum_{n=1}^N \Delta \mathbf{p}_n(k). \quad (26)$$

As it is clear from (26),  $\Delta \bar{\mathbf{p}}(k)$  is the average of the optimal geometric perturbations at the  $k$ -th iteration of the minimization process. Note also that this average coincides with the velocity  $\Delta \bar{\mathbf{p}}(k)$  of the centre of mass of the particle system defined in (19). By exploiting this fact, in the following we define a meaningful optimization problem and use it for optimally define the "centroid" image.

To this end, let  $\mathbb{P}_{k-1}$  be the set  $\mathbb{P}$  defined in (5) containing the values of the parameter vectors resulting after the  $k-1$ -th iteration of the minimization of the non-linear cost function  $\mathcal{E}_0(\mathbb{P}_{k-1}; \mathbf{i}(k-1))$  defined in (10). Then, for the optimal definition of the "centroid" image we can define the following constrained optimization problem:

$$\min_{\mathbf{i}(k)} \mathcal{E}_0(\mathbb{P}_{k-1}; \mathbf{i}(k)) \quad (27)$$

subject to:  $A(k)\mathbf{i}(k) = \mathbf{b}(k)$ .

As we are going to see in the next theorem, the solution of the aforementioned problem differentiates the "centroid" image from the "mean" one for each finite value of  $k$  while it tends to the "mean" as  $k \rightarrow \infty$ , thus ensuring that property  $\mathcal{P}_2$  in (23) holds.

**Theorem 2.1.** *The optimal solution of the optimization problem (27) is given by:*

$$\mathbf{i}(k) = (I - A^\dagger(k)A(k))\mathbf{i}_w(k) + A^\dagger(k)\mathbf{b}(k) \quad (28)$$

where  $I$  is the identity matrix of size  $N_x N_y \times N_x N_y$ ,  $A^\dagger(k)$  the pseudo inverse of matrix  $A(k)$  defined in Eq. (24) and  $\mathbf{b}(k)$  the vector defined in Eq. (25) respectively.

*Proof.* The proof is easy and is left to the reader.  $\square$

Note that in each iteration the optimal ‘‘centroid’’ image is the superposition of two components with each one being associated with an appropriate subspace of the space  $\mathbb{R}^{N_x N_y}$  of the vectorized images. It can be easily proved that the first component coincides with the component  $\mathbf{i}_2(k)$  while the second one with the component  $\mathbf{i}_1(k)$  as they were defined in (Nikolikos et al., 2017). However, we must stress at this point that its computational cost is very low as it compared with the solution proposed in (Nikolikos et al., 2017) where, in each iteration, the Singular Value Decomposition of matrix  $A(k)$  was necessary. Note also that the second component of the ‘‘centroid’’ image ensures that the Condition (21) is satisfied.

An outline of the proposed algorithm follows.

```

Input: Image set  $\mathbb{S}_{i_w}(\mathbb{P})$ , the vector  $\bar{\mathbf{p}}$  and the ROI
Set  $k = 1$ 
repeat
  for  $n = 1 : N$  do
    Compute the Jacobian of the image  $\mathbf{i}_w(\mathbf{p}_n(k-1))$ 
  end
  Use (13, 24, 25) to update  $\bar{\mathbf{i}}_w(k)$ ,  $A(k)$  and  $\mathbf{b}(k)$ 
  Use Eq. (28) to compute the ‘‘centroid’’  $\mathbf{i}(k)$ ;
  for  $n = 1 : N$  do
    Use (11) to compute the optimal perturbations  $\Delta \mathbf{p}_n(k)$  that align image  $\mathbf{i}_w(\mathbf{p}_n(k-1))$  to the ‘‘centroid’’ image  $\mathbf{i}(k)$  and warp the image accordingly
  end
   $k = k + 1$ 
until  $\mathcal{E}_0(\mathbb{P}_{k-1}; \mathbf{i}(k))$  has converged;
Output: Image set  $\mathbb{S}_i$ 

```

Algorithm 1: Outline of the Proposed LS-Centroid Congealing Algorithm.

### 3 REGISTRATION OF MULTI-CONTRAST MR IMAGES

In this section we are going to present the most common different modalities of MR Images. Then, the edge preserving filtering scheme, originally proposed in (Nikolikos et al., 2019), for their preprocessing will be shortly explained.

#### 3.1 Multi-contrast MR Images

Unlike imaging using radiation, in which the contrast depends on the different attenuation of the structures being imaged, the contrast in MR Images depends on the magnetic properties and the number of hydrogen nuclei existing in the area being imaged. The two basic types of MR Images, often referred to as  $T1$  and  $T2$  images, are  $T1$ -weighted and  $T2$ -weighted images. The main difference between those types of MR Images is the timing of the radiofrequency pulse sequences that is used to make them. The timing pulse sequence used for  $T1$  images results in images which highlight fat tissue, while the timing pulse sequence used for making  $T2$  images results in images which highlight fat, as well as, water within the body. Unlike  $T1$  and  $T2$  images, Proton Density ( $PD$ ) images do not display the magnetic characteristics of the hydrogen nuclei, but the number of nuclei in the area being imaged. Finally, magnetic resonance angiography ( $MRA$ ) is a type of MRI that looks specifically at the body’s blood vessels.

In Figure 1 four slices, one for each aforementioned MRI type of images, are shown. It is clear that the different types of MRI images have totally different intensity distributions, a fact that has the same impact as the strong photometric distortions. Thus, the use of intensity based techniques for aligning, either pairwise or groupwise, multi-modal images does not constitute a good choice for the solution of the problem at hand. In order to be able to use such area based techniques, the preprocessing of the images or volumes with a known edge preserving filter was proposed (Nikolikos et al., 2019).

#### 3.2 Self Quotient Images

A powerful image processing based technique achieving invariance to local illumination distortions was proposed in (Wang et al., 2004) that results, in the transformation of the image, to the well known SQI. According to this technique, the SQI is defined as the ratio of a given image to its smoothed version



and aims to construct a shadow invariant representation of the original image. SQI is defined as the ratio of a given image to its smoothed version aiming to construct a brightness invariant representation of the initial image. Note that the invariance of that image's representation holds for all contrast types of MR images and volumes, since for both brighted and no-brighted tissues the ratio effectively removes the brightness effects. To this end, let  $I_\sigma(x)$  be a smoothed version of the image  $I(x)$  that results from its convolution with the isotropic Gaussian kernel  $G_\sigma(x)$ , with the subscript denoting its standard deviation. That is:

$$I_\sigma(x) = I(x) * G_\sigma(x) \quad (29)$$

where “\*” denotes the 2-D convolutional operator. Suppose also that we are given a set of coordinates  $x$  within the image, which consists the target area or target. Then, the Self Quotient Image is defined as follows:

$$Q(x) = \frac{I(x)}{I_\sigma(x)}, \forall x \in T. \quad (30)$$

Note that the deviation of the Gaussian kernel controls the width of the edges in the image defined in Eq. (30). To address the noise as well as the outliers problem from which SQI suffers from we use a hard thresholding procedure. Considering pairwise registration, let  $\sigma_{Q_r}, \sigma_{Q_w}$  be the standard deviations of the vectorized counterparts of SQIs  $Q_r(\cdot)$  and  $Q_w(\cdot)$ , where  $Q_r(\cdot)$  and  $Q_w(\cdot)$  the template and the warped image respectively. Then, we can define the following threshold:

$$T_\mu = \mu \min\{\sigma_{Q_r}, \sigma_{Q_w}\} \quad (31)$$

with  $0 < \mu < 1$  a parameter that can be used to have additional control over the value of threshold  $T_\mu$ . In all experiments we have conducted we set  $\mu = 1/2$ . The SQIs resulting from the application of the above mentioned procedure on the four different contrast type MRI slices that are shown in Figure 1. In the context of the group-wise problem, we calculate the threshold for each pair that consists of an image of the ensemble and the current centroid image. Having filtered out the strong photometric distortions, we can use the above mentioned area based technique for solving the groupwise alignment problem.

## 4 EXPERIMENTS

In this section we are going to present our results by applying the proposed technique in a series of experiments on real as well as artificial data. The first experiment is conducted with data from AR database<sup>2</sup>.

<sup>2</sup><http://www2.ece.ohio-state.edu/aleix/ARdatabase.html>

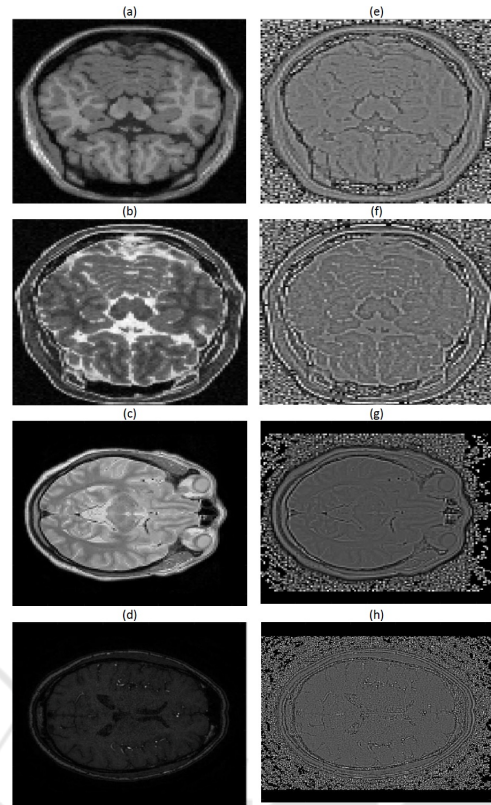


Figure 1: (a)-(d): Original  $T1$ ,  $T2$ ,  $PD$  and  $MRA$  images respectively, (e)-(h): The corresponding SQI's after thresholding for  $T1$ ,  $T2$ ,  $PD$  and  $MRA$  images respectively.

The rest of the experiments are conducted with artificial MRI data obtained from Brainweb Database<sup>3</sup> and real data from IXI Dataset<sup>4</sup>, to test the alignment of images of the same or different modalities. In two experiments we also applied artificial warps to the images. In order to control the strongness of the used warps applied to the initial images, the framework presented in (Baker and Matthews, 2004) was used, with the distortion parameter  $\sigma$  taking various values.

### 4.1 AR Experiment

Since the groupwise alignment solution proposed derives from the one proposed in (Nikolikos et al., 2017), in this experiment we replicated the experiment conducted using geometrically distorted images from AR database, with the distortion parameter  $\sigma$  taking values in the interval  $[1, 10]$  with the values 1 and 10 corresponding to the smallest and strongest geometric distortions respectively. The resulting mean images confirm that the two techniques have the same

<sup>3</sup><https://www.mcgill.ca/bic/software/brainweb-mri-simulator>

<sup>4</sup><https://brain-development.org/ixi-dataset/>



Figure 2: Mean image of 50 images with  $\sigma = 4$  after alignment.

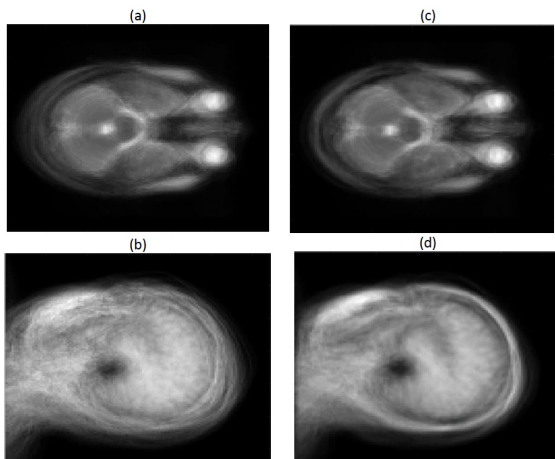


Figure 3: (a): Original mean image of 50  $T_2$  images, (b): Original mean image of 50  $T_1$  images, (c): Mean image of (a) after alignment, (d): Mean image of (b) after alignment.

performance, as we may see in Figure 2, although the proposed closed form solution ensures that the latter is much faster than its predecessor.

## 4.2 MRI Experiments

We conducted a series of experiments with different MRI image modalities, namely  $T_1$ ,  $T_2$ ,  $PD$  and  $MRA$ .

### 4.2.1 Unimodal Alignment

First, we aim to align images from IXI Dataset containing the same slice, of the same modality, from 50 different subjects. In Figure 3 we can see the mean image in  $T_1$  and  $T_2$  cases.

It is obvious in Figure 3 that the contour of the mean image after alignment is much clearer and more defined.

### 4.2.2 Multimodal Alignment in Artificial Data

In this experiment we align images from Brainweb Database, where we add small artificial warps of  $\sigma = 1$ , aligning then across the same slice different modalities  $T_1$ ,  $T_2$  and  $PD$ . In Figures 4 and 5 we see the mean image for random slices, as well as the three aligned images in each case.

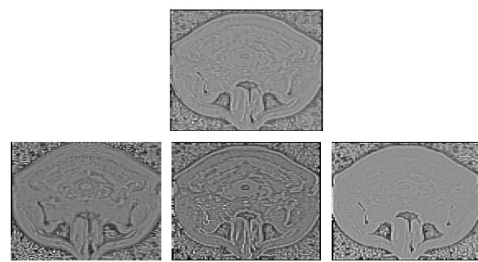


Figure 4: Middle Top Image: Mean quotient image of three below images after alignment, Bottom Row:  $T_1$ ,  $T_2$  and  $PD$  quotient images respectively.

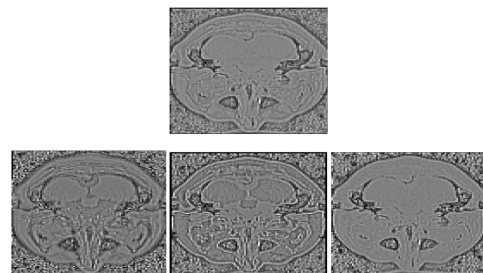


Figure 5: Middle Top Image: Mean quotient image of three below images after alignment, Bottom Row:  $T_1$ ,  $T_2$  and  $PD$  quotient images respectively.

### 4.2.3 Multimodal Alignment in Real Data

In this experiment we align images from IXI Dataset, aligning them across the same slice different modalities  $T_2$ ,  $MRA$  and  $PD$ . In Figure 6 we see the mean image for random slices from 28 subjects from each modality, while in Figure 7 we can see an example image from each modality,  $T_2$ ,  $PD$ ,  $MRA$  along with their respective quotient images which are obviously the ones that allow multi-modal registration.

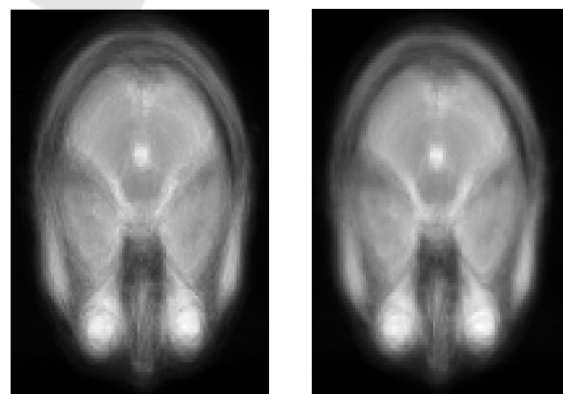


Figure 6: Left Image: Original "mean" image of  $T_2$ ,  $MRA$  and  $PD$  images, Right Image: "mean" image after alignment.

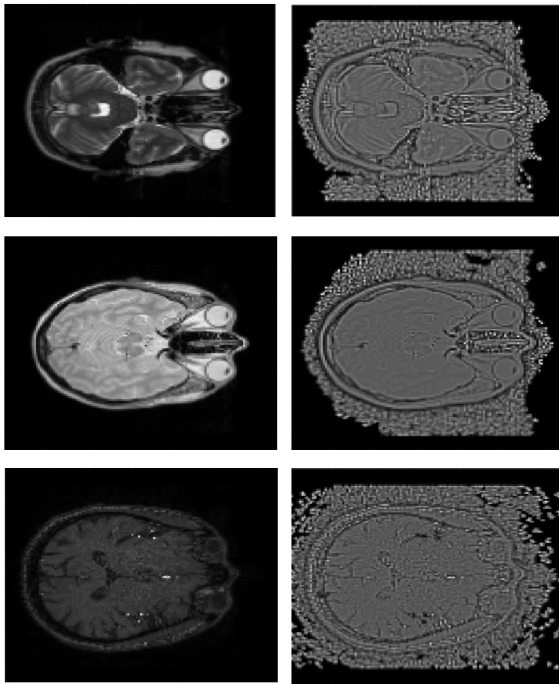


Figure 7: Top Row: *T2* image(left) and the respective quotient image(right), Middle Row: *PD* image(left) and the respective quotient image(right), Bottom Row: *MRA* image(left) and the respective quotient image(right).

## 5 CONCLUSIONS

In this work a recently introduced Least-Squares based groupwise image registration method was improved in terms of its computational cost. This was achieved by optimally defining a sequence of “centroid” images whose limit was the desired but unknown “mean” image for solving the groupwise problem. In addition, the proposed technique was properly adapted for its use in the groupwise registration of multimodal images. The performance of the proposed technique, from its application on a number of experiments, was very good. The extensive evaluation of its performance against other state of the art groupwise registration techniques and its extension for solving the corresponding groupwise volume problem are currently under investigation.

## ACKNOWLEDGEMENTS

This research is implemented through the Operational Program “Human Resources Development, Education and Lifelong Learning” and is co-financed by the European Union (European Social Fund) and Greek national funds.

## REFERENCES

- Baker, S. and Matthews, I. (2004). Lucas-kanade 20 years on: A unifying framework. *International Journal of Computer Vision* 56(3), 221–255.
- Cox, M. (2010). *Unsupervised alignment of thousands of images*. PhD thesis, Queensland University of Technology, Brisbane, Queensland.
- Cox, M., Sridharan, S., Lucey, S., and Cohn, J. (2008). Least squares congealign for unsupervised alignment of images. *CVPR*.
- Cox, M., Sridharan, S., Lucey, S., and Cohn, J. (2009). Least squares congealign for large number of images. *CVPR*.
- Guyader, Jean-Marie, Huizinga, Wyke, Poot, J., D. H., van Kranenburg, Matthijs, Uitterdijk, A., Niessen, W. J., and Klein, S. (2018). Groupwise image registration based on a total correlation dissimilarity measure for quantitative mri and dynamic imaging data. *Scientific Reports*, 8(1):13112.
- Huang, G., Jain, V., and Learned-Miller, E. (2007). Unsupervised joint alignment of complex images. In *ICCV-2007*.
- Huang, G. B., Mattar, M. and Lee, H., and Learned-Miller, E. (2012). Learning to align from scratch. In *Neural Information Processing Systems*.
- Huizinga, W., Poot, D. H. J., Guyader, J.-M., Klaassen, R., Coolen, B. F., van Kranenburg, M., van Geuns, R. J. M., Uitterdijk, A., Polfliet, M., and et al., J. V. (2016). Pca-based groupwise image registration for quantitative mri. *Med Image Anal.*, pages 65–78.
- Learned-Miller, E. (2006). Data driven image models through continuous joint alignment. *IEEE T-PAMI*, 28(2):236–250.
- Liu, Q. and Wang, Q. (2014). Groupwise registration of brain magnetic resonance images: A review. *Journal of Shanghai Jiaotong University (Science)*, 19(6):755–762.
- Nikolikos, N., Lamprinou, N., Boile, A., and Psarakis, E. (2019). Multi-contrast mri volume alignment via ecc maximization. In *BioInformatics and BioEngineering (BIBE)*. IEEE.
- Nikolikos, N., Psarakis, E., and Lamprinou, N. (2017). A new least squares based congealing technique. *Elsevier Pattern Recognition Letters*, 95:58–64.
- Storer, M. and Urschler, M. (2010). Intensity-based congealing for unsupervised joint image alignment. In *ICPR, 2010*.
- Tong, C., Liu, X., Willer, F., and Tu, P. (2009). Automatic facial landmark labelin with minimal supervision. In *CVPR, 2009*.
- Vedaldi, A. and Soatto, S. (2006). A complexity-distortion approach to joint pattern alignment. In *NIPS*.
- Wang, H., Li, S. Z., Wang, Y., and jun Zhang, J. (2004). Self quotient image for face recognition. In *International Conference on Image Processing (ICIP)*, pages 1397–1400. IEEE.
- Xue, Y. and Liu, X. (2012). Image congealign via efficient feature selection. *Applications of Computer Vision (WACV)*.
- Zollei, L. (2006). *A Unified Information Theoretic Framework for Pair- and Group-wise Registration of Medical Images*. PhD thesis, MIT Computer Science and Artificial Intelligence Laboratory.